AIAA 2016-1880
AIAA SciTech
4-8 January 2016, San Diego, California, USA
54th AIAA Aerospace Sciences Meeting

Level-educed Wavepacket Representation of Noise Radiation from a High-performance Military Aircraft

Tracianne B. Neilsen,[1] Kent L. Gee,[2] Blaine M. Harker[3]
Brigham Young University, Provo, UT, 84602

and

Michael M. James[4]
Blue Ridge Research and Consulting, LLC, Asheville, NC, 28801

An analytical, wavepacket-based model has been applied for the first time to high-performance, military aircraft noise. Ground-based acoustical measurements were made of a tethered high-performance military aircraft with one engine cycling through four engine conditions. The resulting spectra have been decomposed into fine and large-scale similarity spectral components. The spatial distribution of the large-scale similarity spectrum decomposition provides the opportunity to extract level-based, data-educed wavenumber spectra associated with pressure fluctuations on a cylinder concentric with the nozzle and an estimation of the convective speed as a function of frequency and engine condition. The amplitudes of the data-educed wavenumber spectra are compared with spatial Fourier transform of an analytical wavepacket model, and a simulated annealing algorithm is employed to find modeling parameters that minimize the difference. The frequency-dependent wavepacket shapes obtained from the optimizations follow the expected trend of contracting in length as frequency increases, although each extend approximately the same number of wavelengths. The optimized wavenumber spectra predict the spatial distribution of the Mach wave radiation associated with the large-scale turbulent mixing noise. This wavepacket study is a step towards producing an equivalent source representation of noise from tactical gas turbine engines to guide future noise environment modeling efforts.

Nomenclature

a_n	=	stochastic random function
A	=	normalization factor
A_j	=	scaled normalization factor
A_n	=	axial wavenumber spectrum amplitude
b_1	=	length scale of growth of axial wavepacket
b_2	=	length scale of decay of axial wavepacket
c	=	ambient sound speed
D_j	=	jet nozzle diameter
ETR	=	engine thrust request
f	=	frequency
F_n	=	azimuthal mode contributions
E	=	cost function
g_1	=	rate of growth of axial wavepacket
g_2	=	rate of decay of axial wavepacket

[1] Part-Time Assistant Professor, Dept. of Physics and Astronomy, N283 ESC, AIAA Member.
[2] Associate Professor, Dept. of Physics and Astronomy, N283 ESC, AIAA Senior Member.
[3] Graduate Student, Dept. of Physics and Astronomy, N283 ESC, AIAA Student Member.
[4] Senior Principal Engineer, 29 N Market St, Suite 700, AIAA Member.

G_n = axial wavenumber spectrum
$\boldsymbol{k}$ = wavenumber vector
k = acoustic wavenumber
k_z = axial wavenumber
k_r = radial wavenumber
$L_{w,\mathrm{far}}$ = far-field levels due to a wavepacket
$\boldsymbol{m}$ = vector containing the modeling parameters
M_c = convective Mach number
n = azimuthal mode number
OASPL= overall sound pressure level
p = acoustic pressure
p_0 = wavepacket axial shape
$\hat{p}_0$ = axial wavenumber spectum
$\hat{P}_0$ = self-similar axial wavenumber spectrum
p_{ref} = reference pressure
p_w = pressure modeled by a wavepacket
p_m = pressure modeled by a monopole
P_n = radially dependent wavenumber/frequency spectrum,
Q = monopole source strength
r_0 = radius of the nozzle
r = radius in cylindrical coordinates
R = radius in spherical coordinates
S = spectral density
$S_{w,\mathrm{far}}$ = modulus of the far-field estimate of the square pressure
St = Strouhal number
t = time
U_c = convective velocity
U_j = jet velocity
z = axial distance
β = angle relative to engine inlet
ϵ = frequency-dependent amplitude
ϕ = azimuthal angle
θ = polar angle
λ = wavelength
ρ_j = jet density
ω = angular frequency

I. Introduction

Wavepacket representations of jet noise strive to provide a model consistent with linear stability theory of the mean flow[1,2] that incorporates features of the highly directional turbulent mixing noise.[3,4,5] A wavepacket has been described as a spatially extended source characterized by an axial amplitude distribution that grows, saturates and decays, an axial phase relationship that produces directional noise,[6] and correlation lengths longer than the integral length scales of the turbulence.[7] Wavepacket characteristics are found in the turbulent region, the hydrodynamic near field and the acoustic far field.[3] However, depending on the convective Mach number (relative to the ambient sound speed), a wavepacket describes either primarily convectively subsonic sound radiation or the highly directional Mach wave radiation (convectively supersonic). The goal is to create a wavepacket model of jet noise that can be employed in future noise environment modeling and noise reduction efforts.

Wavepacket investigations of jet noise have been conducted using measurements in the turbulent region, hydrodynamic near field, and acoustic far field of laboratory-scale jets. Beginning with Mollo-Christensen,[8] wavepacket-like features have been observed in near-field pressure measurements. More recently, visualization methods have been used to estimate wavepacket properties associated with the turbulent flow, as e.g., in Ref. 9.

Arrays of microphones in the hydrodynamic near field have been used to detect linear instability waves and connect them to near-field pressure wavepackets[10-13] Methods for linking the wavepackets educed from the near-field data to the far-field sound radiation have also shown promise.[6,7,14]

Based on linear stability theory,[1,2] techniques have been proposed to use far-field measurements to infer wavepackets that model the radiating portion of the pressure fluctuations.[15] Morris[16] and Papamoschou[17,18] present two methods for obtaining wavepacket representations with the same goal: for a single frequency, connect far-field measured spectral levels with a wavepacket representation of the source radiated pressure projected on a near-field cylinder centered on the jet centerline. Morris[16] showed how the spatial distribution of levels from the large-scale similarity spectra decomposition of far-field spectra yield frequency-dependent, axial wavenumber spectra for a range of jet velocities. Papamoschou proposed an analytical wavepacket model to predict far-field sound levels. Because both methods begin with far-field noise, information is not available about the nonradiating, evanescent components of the turbulent pressure variations in the hydrodynamic near field. Nevertheless, the acoustic field contains information sufficient to obtain an equivalent wavepacket model representative of the levels of the propagating noise.

The initial application of the wavepacket ansatz to full-scale, military aircraft noise begins with the procedure described by Morris[16] for obtaining the azimuthally-averaged, axial wavenumber spectral amplitudes. The investigation into a wavepacket representation for full-scale military jet noise continues by using the data-educed wavenumber spectra from a ground-based microphone array in the vicinity of an F-22A Raptor.[19] The data-educed wavenumber spectra are used to estimate convective velocities and to find frequency-dependent analytical wavepackets that model the large-scale turbulent mixing noise. The five-parameter analytical wavepacket model described in Papamoschou[17] has been employed in this preliminary study. The Fourier transform of the model's complex wavepacket amplitude distribution yields an analytical wavenumber spectrum, which is compared to the data-educed wavenumber spectra in the optimization. To provide insights into the relative uncertainty in the parameter estimates obtained by the optimization, a study concerning how the wavepacket parameters relate to features in the analytical wavenumber spectrum is presented. Finally, the analytical wavenumber spectra obtained from the optimizations at different frequencies can be used to estimate the far-field levels. This initial evaluation of the ability of the wavepacket ansatz to yield the levels measured in the vicinity of a high-performance military aircraft indicates there is potential in this equivalent acoustic source representation and points towards modifications of the wavepacket model that will enhance the prediction.

II. Background

In this paper, two methodologies are linked together and expanded to create a frequency-dependent wavepacket model for noise near a high-performance military aircraft. First, the measured spectra are decomposed into the two similarity spectra for turbulent mixing noise given by Tam *et al.*[22] Following the derivations in Refs. 20, 21, and 16, the spatial dependence of levels associated with the large-scale similarity spectrum provides estimates of the axial wavenumber spectrum as a function of frequency. These data-educed wavenumber spectra are compared to the spatial Fourier transforms of analytical wavepacket models given by Papamoschou.[17] The corresponding wavenumber spectra can be used to obtain numerical estimates of the far-field noise levels. These theoretical developments are presented in this section. The nomenclature has been modified slightly from the original presentations to provide a consistent framework tying the methods together.

Before beginning the derivations, the relationship between the acoustic, axial, and radial wavenumbers needs to be considered. For a sound wave of angular frequency ω traveling in a medium with wave speed c, the magnitude of the acoustic wavenumber is $k = \omega/c$, and the wavenumber vector, $\boldsymbol{k}$, points in the direction the wave is traveling. In cylindrical coordinates, the angle at which the wavenumber vector points relative to the z axis is $\theta = \tan^{-1}(k_r/k_z)$, where the z and r components of the acoustic wavenumber vector are $k_z = k\sin\theta$ and $k_r = k\cos\theta$. The wavenumber associated with radial direction, $k_r = \pm\sqrt{k^2 - k_z^2}$, is real if $|k_z| \leq \omega/c$ and, in such cases, corresponds with waves propagating outward from the source. Such wavenumbers are called sonic (when equal) or supersonic, signifying trace wavenumber matching in the axial direction. Note that $k_r = \pm\sqrt{k^2 - k_z^2}$ is imaginary when $k_z > k$. The positive or negative sign associated with the square root is chosen such that when $k_z > k$ (subsonic wavenumbers), the associated wavenumber components decay evanescently with radial distance. Because our measurements are not in the hydrodynamic near field (i.e., more than a half wavelength away at frequencies of interest[19]), the k_z values represented in the axial wavenumber spectra are restricted to propagating waves with supersonic axial wavenumbers: $|k_z| \leq \omega/c$.

A. Level-educed Wavenumber Spectrum

One model for jet noise postulates that sound radiated from the jet exhaust plume is generated by turbulent mixing noise from fine-scale and large-scale turbulent structures. Tam *et al.*[22] used an extensive database of laboratory-scale jet data and found a similarity spectrum associated with each kind of turbulent mixing noise. To the sideline direction, the fine-scale similarity (FSS) spectrum matches the radiated noise spectrum for a range of jet operating conditions. Similarly, the large-scale similarity (LSS) spectrum approximates the spectral shape in the maximum sound radiation direction, often referred to as the Mach cone. In between these two regions, a combination of the FSS and LSS spectra is needed to account for the spectral shape. Examples of the decomposition of measured jet noise spectra into FSS and LSS spectral components are found in Morris,[16] Tam *et al.*,[4,22-24] and Viswanathan,[25-27] for laboratory-scale jets and for military aircraft engines in Schlinker *et al.*[28] and Neilsen *et al.*[29-30] When this spectral decomposition is performed for an array of microphones, the spatial variation in the levels associated with the LSS component at frequency f can be tied to the wavepacket ansatz.

The connection between wavenumber spectral amplitudes and the measured spectral density begins with the solution to the wave equation for pressure fluctuations from a wavepacket represented as a normalized eigenfunction expansion. Next, an expression for the coaxial pressure fluctuations on a cylindrical surface due to stochastic jet noise leads to an expression for the autocorrelation. The ensemble-averaged autocorrelation of these pressure fluctuations are related to those of the noise exiting the nozzle due to the self-similar nature of the turbulence. Each step is now explained in detail.

The three-dimensional wave equation in cylindrical coordinates is

$$\frac{\partial^2 p}{\partial t^2} - c^2\left(\frac{\partial^2 p}{\partial r^2} + \frac{1}{r}\frac{\partial p}{\partial r} + \frac{1}{r^2}\frac{\partial^2 p}{\partial \phi^2} + \frac{\partial^2 p}{\partial z^2}\right) = 0.$$

The general solution in cylindrical coordinates, $p(r,\phi,z,t)$, can be represented in terms of its Fourier transforms with respect to time, t, and axial distance, z, as well as a Fourier series in the azimuthal angle, ϕ:

$$p(r,\phi,z,t) = \frac{1}{(2\pi)^3}\sum_{n=-\infty}^{n=\infty}\int_{-\infty}^{\infty}\int_{-\infty}^{\infty} P_n(r,k_z,\omega)e^{i(n\phi+kz-\omega t)}d\omega dk_z, \qquad \textbf{(1)}$$

with ω as the angular frequency and k_z as the axial wavenumber. From the wave equation, the corresponding ordinary differential equation for $P_n(r,k_z,\omega)$, the radially dependent wavenumber/frequency spectrum, is

$$\frac{d^2 P_n}{dr^2} + \frac{1}{r}\frac{dP_n}{dr} + \left(\omega^2 - k_z^2 - \frac{n^2}{r^2}\right)P_n = 0.$$

The general solution is

$$P_n(r,k_z,\omega) = A_n(k_z,\omega)H_n^{(1)}(k_r r), \qquad \textbf{(2)}$$

where $H_n^{(1)}(\xi)$ is the Hankel function of the first kind of order n and argument ξ, and k_r is the radial wavenumber. The amplitude $A_n(k_z,\omega)$ constitute the variations of the acoustic pressure as a function of axial wavenumber and frequency on a cylinder a distance r from the jet centerline.

From previous work,[20-21] it was found that the random or stochastic nature of jet noise causes the pressure fluctuations on a cylindrical surface coaxial with the jet to be broadband and nondeterministic. The radially dependent wavenumber/frequency spectrum of the pressure fluctuations of the nth azimuthal mode on a cylindrical surface of radius r_0 can be expressed in terms of a modal series expansion as

$$P_n(r_0,k_z,\omega) = a_n(\omega)G_n(k_z,\omega), \qquad \textbf{(3)}$$

where $a_n(\omega)$ is a stochastic random function of frequency and $G_n(k_z,\omega)$ are normalized axial eigenfunctions.

By equating Eq. (2) and Eq. (3) at $r = r_0$, an expression for the amplitude $A_n(k_z, \omega)$ is obtained, such that the radially dependent wavenumber/frequency spectrum of the pressure fluctuations in terms of the axial eigenfunctions is

$$P_n(r, k_z, \omega) = \frac{a_n(\omega) H_n^{(1)}(k_r r)}{H_n^{(1)}(k_r r_o)} G_n(k_z, \omega). \tag{4}$$

The pressure fluctuations at $r \geq r_o$ is obtained by taking the inverse Fourier transforms of Eq. (4) with respect to ω and k_z:

$$p(r, \phi, z, t) = \frac{1}{(2\pi)^3} \sum_{n=-\infty}^{n=\infty} \int_{-\infty}^{\infty} \int_{-\infty}^{\infty} \frac{a_n(\omega) H_n^{(1)}(k_r r)}{H_n^{(1)}(k_r r_o)} G_n(k_z, \omega) e^{i(n\phi + kz - \omega t)} d\omega dk_z. \tag{5}$$

At this point, the eigenfunctions $G_n(k_z, \omega)$ can be identified as the frequency-dependent axial wavenumber spectra, hereafter referred to as the wavenumber spectrum. Based on Eq. (5), the ensemble average of the autocorrelations of these pressure fluctuations is

$$\langle p(r, \phi, z, t) p(r, \phi, z, t + \tau) \rangle = \frac{1}{(2\pi)^6} \sum_{n=-\infty}^{n=\infty} \sum_{n'=-\infty}^{\infty} \int_{-\infty}^{\infty} \int_{-\infty}^{\infty} \int_{-\infty}^{\infty} \int_{-\infty}^{\infty} \langle a_n(\omega) a_{n'}(\omega') \rangle \frac{H_n^{(1)}(k_r r)}{H_n^{(1)}(k_r r_o)} \frac{H_{n'}^{(1)}(k_r' r)}{H_{n'}^{(1)}(k_r' r_o)}$$

$$\cdot\, G_n(k_z, \omega)\, G_{n'}(k_z', \omega) e^{i((n-n')\phi + (k_z - k_z')z - (\omega - \omega')t)}\ d\omega d\omega' dk_z dk_z'.$$

In Refs. [16, 20-21], the argument is made that the instability waves associated with the large turbulent structures have no intrinsic characteristic time and length scales, i.e., they are self-similar. This is equivalent to saying that they are excited by white noise at the nozzle exit plane, $z = 0$, in which case, the autocorrelation functions contain delta functions in both polar angle and time. Using the notation of Morris,[16] this yields

$$\left\langle \frac{p(r_o, \phi, 0, t)}{\rho_j u_j^2} \frac{p(r_o, \phi + \chi, 0, t + \tau)}{\rho_j u_j^2} \right\rangle = A^2 \rho_j^2 U_j^3 D_j\ \delta(\chi)\delta(\tau),$$

where D_j is the diameter of the jet nozzle, ρ_j and U_j are the density and speed of the jet, and A^2 is a normalization factor. This expression of the autocorrelation due to the self-similar nature of the turbulence can be connected to the stochastic property of the function $a_n(\omega)$ by repeated use of the Fourier transform and application of the normalization such that

$$\langle a_n(\omega) a_{n'}(\omega') \rangle = A^2 \rho_j^2 U_j^3 D_j\ \delta(\omega + \omega') \delta_{n,-n'}$$

where $\langle * \rangle$ denotes the ensemble average, $\delta_{n,-n'}$ is the Kronecker delta (which equals 1 when $n = -n'$ and equals zero otherwise) and $\delta(\omega + \omega')$ is the Dirac delta function:

$$\delta(\omega - \omega') = \frac{1}{2\pi} \int_{-\infty}^{\infty} \mathrm{e}^{ip(\omega - \omega')} dp.$$

The sifting properties of the Delta functions and the relationship between the positive and negative sides of the Fourier transforms lead to a simpler expression for the autocorrelation at position (r, ϕ, z) relative to pressure fluctuations on a cylinder of radius r_o, namely

$$\langle p(r, \phi, z, t) p(r, \phi, z, t + \tau) \rangle = \frac{A^2}{2\pi^2} \rho_j^2 U_j^3 D_j \sum_{n=-\infty}^{\infty} \int_{-\infty}^{\infty} |F_n(r, z, \omega)|^2\ e^{-i\omega\tau} d\omega,$$

where

$$F_n(r,z,\omega) = \int_{-\infty}^{\infty} G_n(k_z,\omega)\,\frac{H_n^{(1)}(k_r r)}{H_n^{(1)}(k_r r_o)}\,e^{ik_z z}dk_z. \tag{6}$$

The Fourier transform with respect to time of the autocorrelation is the autospectral density,

$$S(r,z,\omega) = \int_{-\infty}^{\infty} \langle p(r,\phi,z,t)p(r,\phi,z,t+\tau)\rangle\, e^{i\omega\tau}d\tau,$$

which can be expressed as a sum of the modal contributions, $F_n(r,z,\omega)$ in Eq. (6), by

$$S(r,z,\omega) = \frac{A^2}{2\pi}\rho_j^2 U_j^3 D_j \sum_{n=-\infty}^{\infty} |F_n(r,z,\omega)|^2. \tag{7}$$

Thus, the spectral density at a location (r,z) and angular frequency, ω, may be expressed as the sum over azimuthal modes of the inverse Fourier transform with respect to k_z (from Eq. (6)) of the axial wavenumber spectrum (in Eq.(4)).

Although there is a summation over n in Eq. (7), use of only the $n = 0$ term is often a good approximation, especially for lower frequency noise from axisymmetric jets.[16,21,23] Restriction to only the $n = 0$ term is also applied if the measurements span a limited azimuthal aperture so as to lack sufficient information to estimate the contributions from higher-order azimuthal modes ($n > 0$). In this case, an azimuthally averaged result is obtained. Thus, the measured spectral density, $S(r,z,\omega)$, can be used to find the scaled magnitude of $G_0(k_z,\omega)$, the axial eigenfunction of order zero.

The connection between $G_0(k_z,\omega)$ and $S(r,z,\omega)$ is more straightforward if a transformation is made from cylindrical to spherical coordinates using $z = R\cos(\theta)$ and $r = R\sin(\theta)$, where R is the distance from the origin to the point at (r,z), and θ is the angle relative to the z axis. In addition, the Hankel function of the first kind can be approximated, for large arguments, by its asymptotic form:

$$H_0^{(1)}(\zeta) \to \sqrt{\frac{2}{\pi\zeta}}\,e^{i\left(\zeta-\frac{\pi}{4}\right)} \text{ as } |\zeta| \to \infty. \tag{8}$$

With these modifications, the integral for $F_0(R,\theta,\omega)$ in Eq. (6) is evaluated by the method of stationary phase to obtain

$$F_0(R,\theta,\omega) = -\frac{2i}{R}\frac{G_0(k_z,\omega)}{H_0^{(1)}(k_r r_o)}\,e^{i\omega R/c_0}. \tag{9}$$

Inserting the expression in Eq. (9) into Eq. (7) yields the relationship

$$S(R,\theta,\omega) = \frac{A^2}{2\pi}\rho_j^2 U_j^3 D_j \left|\frac{2}{R}\frac{G_0(k_z,\omega)}{H_0^{(1)}(k_r r_o)}\right|^2.$$

This expression can be rewritten as

$$\frac{A^2 \rho_j^2 U_j^3 |G_0(k_z,\omega)|^2}{D_j^2} = \frac{\pi}{2}\left(\frac{R}{D_j}\right)^2 \left|H_0^{(1)}(k_r r_0)\right|^2 \frac{S(R,\theta,\omega)}{D_j}. \tag{10}$$

The quantities on the right-hand side of Eq. (10), (R, D_j, r_0, $S(R,\theta,\omega)$, and k_r) are measured quantities. The left-hand side is the squared amplitude of the wavenumber spectrum associated with the $n = 0$ azimuthal mode scaled by jet operating parameters. In the case of installed engines, the jet operating parameters ρ_j and U_j are not available. Thus, we rewrite Eq. (10) as

$$\frac{A_j^2}{D_j^2}|G_0(k_z,\omega)|^2 = \frac{\pi}{2}\left(\frac{R}{D_j}\right)^2 \left|H_0^{(1)}(k_r r_o)\right|^2 \frac{S(R,\theta,\omega)}{D_j}, \tag{11}$$

where $A_j = A\rho_j U_j^{3/2}$ depends on the jet operating conditions. This expression yields data-educed estimates of the spatial Fourier transform of the wavepacket associated with the $n = 0$ azimuthal mode on a cylindrical surface concentric with the nozzle exit to the measurement-derived LSS spectral amplitudes in $S(R,\theta,\omega)$.

B. Analytical Wavepacket Model

One approach to wavepacket modeling of jet noise is to define an analytical wavepacket shape, and its wavenumber spectrum, that can be used to predict far field levels of the radiated field. The first step is to define a pressure fluctuation, referred to as a wavepacket, on cylindrical surface at $r = r_0$, of angular frequency ω and azimuthal mode number n, as

$$p_w(n, r_0, z, \phi, t) = p_0(z) e^{-i\omega t + in\phi}\ , \tag{12}$$

where ϕ is the azimuthal angle, t is time, and z is the distance from the jet nozzle exit plane. The wavepacket axial shape is $p_0(z)$ is composed of an amplification-decay amplitude envelope and an oscillating portion: $p_0(z) = |p_0(z)|e^{i\alpha z}$, where $\alpha = \omega/U_c$ is the wavenumber associated with the peak in the wavenumber spectrum and is related to the convective speed U_c.

Although there are many options for an amplitude envelope, the wavepacket axial shape defined by Papamoschou in Eq. [35] of Ref. [17], is implemented in our initial investigation into the ability of a wavepacket to represent the turbulent mixing noise associated with the large-scale turbulent structures. The candidate wavepacket model is

$$p_0(z) = \tanh\left[\left(\frac{z}{b_1}\right)^{g_1}\right]\left\{1 - \tanh\left[\left(\frac{z}{b_2}\right)^{g_2}\right]\right\} e^{i\alpha z}\,. \tag{13}$$

The parameters of the first hyperbolic tangent term, b_1 and g_1, control the length scale and the rate of the growth of the wavepacket amplitude. Similarly, b_2 and g_2 dictate the length scale and rate of the decay. Some examples of the real part of p_0 for different combinations of the four parameters $[b_1, b_2, g_1, g_2]$ are displayed in Figure 1 to illustrate the effect they have on the axial amplitude distribution. Each wavepacket is normalized such that the maximum value of $|p_0(z)|$ is unity in each case. The wavepackets in the first row of Figure 1 have different values of $b_1$which facilitates the observation that the location of the first oscillation moves to larger z as b_1 increases up to the value of b_2. However, once $b_1 > b_2$, the shape of the wavepacket does not appear to change significantly. On the second row, b_2 is varied such that an increase in the parameter delays the onset of the oscillations and, in effect, shortens the wavepacket. Similarly, an increase in g_2 shortens the decay and thus the extent. The bottom row of wavepackets in Figure 1 illustrates its relationship to the convective wavenumber, α, for three values of the convective speed U_c: an increase in the wavenumber produces additional oscillations within in the wavepacket. These parameters provide the capability of finely adjusting the wavepacket model, and an understanding of their impact to the overall shape is necessary to interpret comparisons.

Each axial wavepacket shape has a corresponding wavenumber spectrum: $\hat{p}_0(k_z) = \mathcal{F}[p_0(z)]$. Normalized wavenumber spectra for the cases in Figure 1 are displayed in Figure 2. The maximum value of k_z in the wavenumber spectrum is inversely proportional to the distance between the points at which the wavepacket amplitude is defined. Comparisons between the plots in Figure 2 gives an indication of how changes in the wavepacket modeling parameters affect the wavenumber spectrum. Larger values of b_1 and b_2 create a wider wavepacket and thus a narrower spectrum. However, there is not a significant change in spectral shape for cases with $b_1 > b_2$. For $g_2 > g_1$ (on the bottom row of Figure 2), the spectral rolloff for small $k_z D_j$ is less smooth,. In addition, a low convective speed, and, hence, a large convective wavenumber, has a much broader spectrum than the others. While not a comprehensive list of how the parameters affect the spectrum, the examples provided highlight how features of the wavenumber spectrum can be tied to the wavepacket model. These analytical wavenumber spectra can be compared to data-derived ones to obtain a wavepacket model for full-scale jet noise. In practice, estimates of the modeling parameters are found by a simulated annealing algorithm based on minimizing the least-squares error between the two spectra. This is described further in Section II.D.

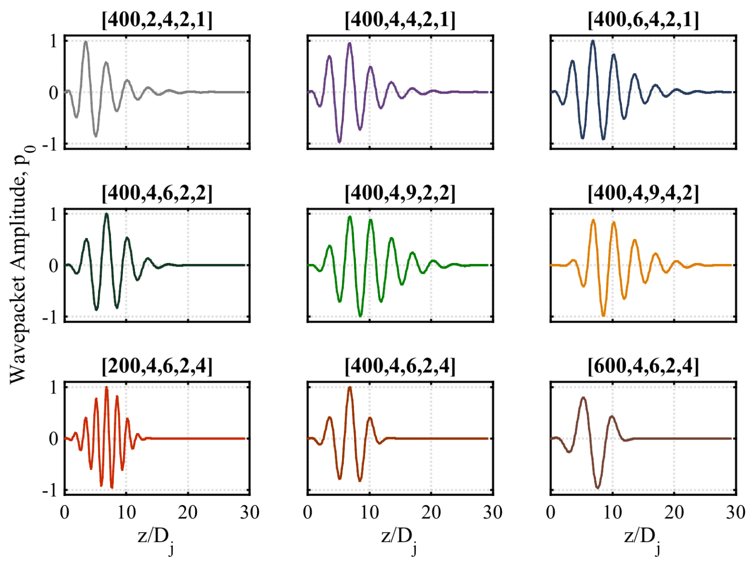

Figure 1. Wavepacket shapes. ***Examples of the real parts of the axial wavepacket shapes at 250 Hz for the parameters listed above each plot:*** $[U_c, b_1, b_2, g_1, g_2]$.

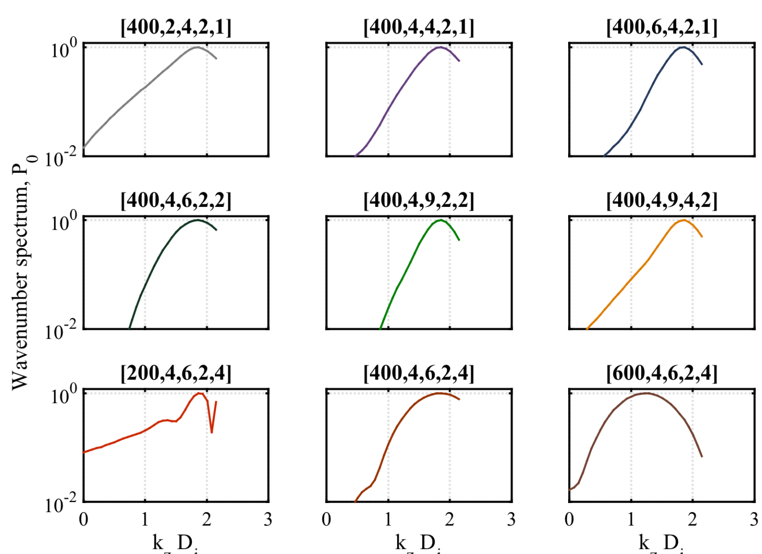

Figure 2. Wavenumber spectra. *The wavenumber spectra corresponding to the wavepacket shapes shown in Figure 1. The modeling parameters are listed above each plot:* $[\boldsymbol{U_c}, \boldsymbol{b_1}, \boldsymbol{b_2}, \boldsymbol{g_1}, \boldsymbol{g_2}]$.

C. Far-field levels

Once an estimated wavenumber spectrum is obtained at each frequency of interest, both Morris[16] and Papmoschou[17] describe the connection between the wavenumber spectrum and modeling the far field sound pressure levels. Beginning with Eq. (5), the pressure, for $r \geq r_o$, is given by the inverse Fourier transform of the wavenumber spectrum associated with a single angular frequency ω:

$$p_w(n,r,\phi,z,t) = \frac{1}{2\pi} e^{-i\omega t + in\phi} \int_{-\infty}^{\infty} \hat{p}_0(k_z) \frac{H_n^{(1)}(k_r r)}{H_n^{(1)}(k_r r_o)} e^{ik_z z} dk_z.$$

This integral can be divided into two parts corresponding with subsonic and supersonic wavenumbers:

$$p_{w,\mathrm{sub}}(n,r,\phi,z,t) = \frac{1}{2\pi} e^{-i\omega t + in\phi} \int_{|k_z|>\omega/c_0} \hat{p}_0(k_z) \frac{H_n^{(1)}(k_r r)}{H_n^{(1)}(k_r r_0)} e^{ik_z z} dk_z$$

$$p_{w,\mathrm{sup}}(n,r,\phi,z,t) = \frac{1}{2\pi} e^{-i\omega t + in\phi} \int_{-\omega/c_0}^{\omega/c_0} \hat{p}_0(k_z) \frac{H_n^{(1)}(k_r r)}{H_n^{(1)}(k_r r_0)} e^{ik_z z} dk_z \qquad \textbf{(14)}$$

Using the far-field approximation in Eq. (8), the equation in Eq. (14) yields an expression for the pressure at far-field position in spherical coordinates (R, θ, ϕ) due to the supersonic portions of the pressure fluctuations that propagate to the far field:

$$p_{w,\mathrm{far}}(n,R,\theta,\phi,t) = -\frac{i}{\pi R} \frac{\hat{p}_0(k_z)}{H_n^{(1)}(k_r r_0)} e^{ikR} e^{-i\omega t + in\phi}, \qquad \textbf{(15)}$$

where R is the distance of the observer from the origin, and θ is the angle from the wavepacket (jet) axis, z, and ϕ is the azimuthal angle.

When using the analytical wavepacket model, such as those in Papamoschou,[17-18] it is convenient to represent $\hat{p}_0(k_z)$ in a self-similar form:

$$\hat{p}_0(k_z) = \frac{\epsilon(\omega) U_c}{\omega} \hat{P}_0\left(\frac{k_z U_c}{\omega}\right).$$

$\hat{P}_0\left(\frac{k_z U_c}{\omega}\right)$ is a self-similar version of the wavenumber spectrum, and $\epsilon(\omega)$ is a frequency-dependent amplitude. With this assumption, the far field pressure from the wavepacket becomes

$$p_{w,\mathrm{far}}(n,R,\theta,\phi,\omega,t) = -\frac{i}{\pi R} \frac{\epsilon(\omega) U_c}{\omega} \frac{\hat{P}_0\left(\frac{k_z U_c}{\omega}\right)}{H_n^{(1)}(k_r r_0)} e^{ikR} e^{-i\omega t + in\phi},$$

with all the ω dependence explicitly indicated. This can be simplified to

$$p_{w,\mathrm{far}}(n,R,\theta,\phi,\omega,t) = -\frac{i}{\pi R} \frac{\epsilon(\omega) U_c}{\omega} \frac{\hat{P}_0(M_c \cos\theta)}{H_n^{(1)}\left(\frac{\omega}{c} r_0 \sin\theta\right)} e^{ikR} e^{-i\omega t + in\phi},$$

because $k_r = k\sin\theta$, $k_z = k\cos\theta$, and $kU_c/\omega = U_c/c = M_c$. The modulus of the squared pressure can be expressed as

$$S_{w,\mathrm{far}}(n,R,\theta,\phi,\omega)=\left(\frac{\epsilon(\omega)U_c}{\pi R\omega}\right)^2\left|\frac{\hat{P}_0(k_z)}{H_n^{(1)}\left(\frac{\omega}{c}r_0\sin\theta\right)}\right|^2. \quad \textbf{(16)}$$

The sound pressure level, in decibels, predicted at this far-field location due to the wavepacket is

$$L_{w,\mathrm{far}}(n,R,\theta,\phi)=10\log\left(\frac{\left|S_{w,\mathrm{far}}(n,R,\theta,\phi)\right|^2}{p_{\mathrm{ref}}^2}\right), \quad \textbf{(17)}$$

where $p_{\mathrm{ref}} = 20\ \mu\mathrm{Pa}$. These predicted levels can be compared to measured levels to evaluate the validity of a wavepacket model for jet noise.

Although this representation of the far field due to the wavepacket is a function of angle from the jet axis, Papamoschou [17] found it necessary to add a monopole to capture the directivity of the jet noise to the sideline of the nozzle exit (large polar angles). The monopole at the origin produces a field $p_m(R,t)=\frac{Q}{R}e^{-i\omega t+ikR}$. Combining this monopole and the far-field pressure from the wavepacket yields square pressure amplitudes of

$$S_{\mathrm{mod}}=\mathrm{S}_{\mathrm{w,far}}+\left(\frac{Q}{R}\right)^2.$$

A monopole is not included in the far- field level predictions in this paper; only the levels of the Mach wave radiation are modeled.

D. Analytical Wavepacket Eduction

The overall goal of this work is to find frequency-dependent, analytical wavenumber spectra that match the data-educed wavenumber spectra via optimization. A simulated annealing algorithm is used to find modeling parameters that minimize the difference in the wavenumber spectra. However, because not all parameters are equally important in determining the quality of the match, a sensitivity study highlights the manner in which the analytical wavenumber spectrum shapes relate to changes in the modeling parameters. This is illustrated in Figure 3 for a specific example of a data-educed wavenumber spectrum where the plotted k_z values are the supersonic wavenumbers that have real peak angles: $\theta_{\mathrm{peak}}=\cos^{-1}(ck_{z,\mathrm{peak}}/\omega)$.

The first step in this comparison is to use the wavenumber that corresponds to the peak in the data-derived spectrum to estimate convective speed U_c, and consequently α, in Eq. (13). The correct value of U_c is necessary to obtain the same peak in the modeled spectrum. Thus, the U_c is most closely tied to the quality of the agreement between the wavenumber spectra, and the estimate of U_c obtained by the optimization has the smallest uncertainty of the five modeling parameters. To highlight the effect of the remaining four parameters on the shape of the wavenumber spectrum, each parameter is adjusted in turn. The value of parameter b_2 is most closely tied to the width of the wavenumber spectrum near the peak. This is illustrated in the upper left plot of Figure 3, in which b_2 is varied while the other parameters are held fixed. From this, it appears that, for this example, a value of $b_2{\sim}6$, provides the curvature of the peak region of the data-educed wavenumber spectrum (shown as circles). This value of b_2 is held fixed while b_1 is varied in the upper right plot. Changes in b_1 do not dramatically affect the shape of the wavenumber spectrum near the peak but appear, for low values, to introduce a bend. For values of $b_1 > b_2$, the wavenumber spectrum does not change. A value of $b_1 = 1.5$ yields an analytical wavenumber spectrum that most closely matches this example spectrum. The lower left plots in Figure 3 shows that while very low values of g_2 produce a narrower wavenumber spectra, the width near the peak remains the same for g_2 larger than about 2. Larger values of g_2 also introduce a bend in the lower part of the spectra. The lower right plot in Figure 3 shows that g_1 does not significantly change the width of the modeled wavenumber spectra near the peak, but higher values of g_1 wider the overall extent of the spectrum. Values of $g_1 = 3.5$ and $g_2 = 1.7$ appear to match the low level features of the wavenumber spectrum the best. This sensitivity study provides insight into the relative uncertainty of wavepacket modeling parameters obtained from an optimization designed to minimize the difference between data-educed and modeled wavenumber spectra and is used to bound the modeling parameters in the optimization.

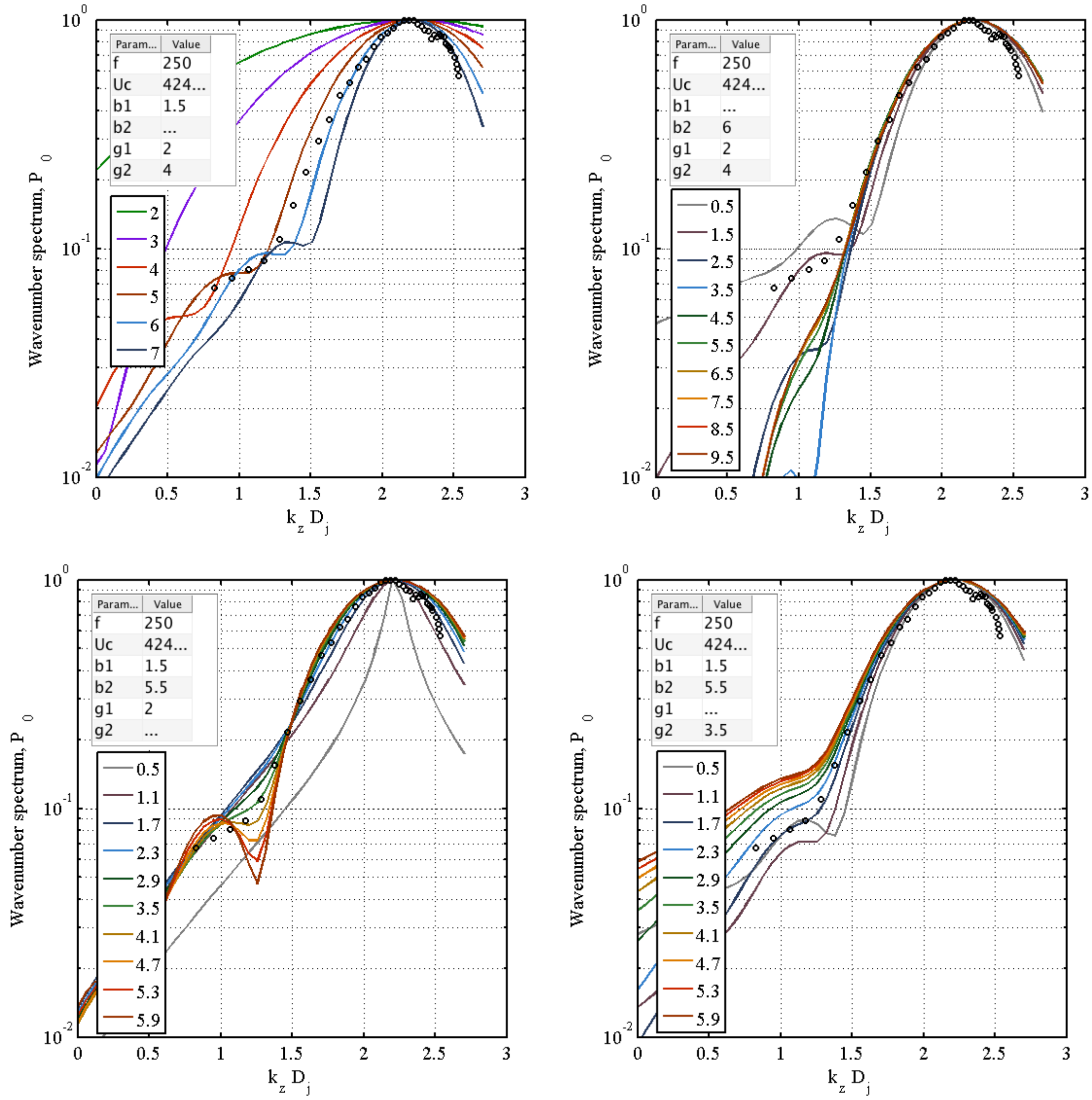

Figure 3. **Parameter sensitivity study.** *Examples of wavenumber spectrum for the parameters indicated in each plot. The parameter with the value indicated by "…" in the upper text box is the one whose values are listed in the legend. An example of a data-educed wavenumber spectrum is shown as circles.*

III. Level-based Analysis

While laboratory-scale studies have investigated the application of a wavepacket ansatz to jet noise, this paper reports the first application of these analyses to full-scale jet noise from a high-performance military aircraft. This study is made possible by the extensive set of noise measurements in the vicinity of an F-22 made jointly by the Air Force Research Laboratory, Blue Ridge Research and Consulting, LLC, and Brigham Young University. One of the engines on the tied-down F-22 was sequentially operated at four engine conditions: idle, intermediate (80% ETR), military (100% ETR), and afterburner, while the other engine was held at idle. An array of 50 GRAS 6.35-mm and 3.18-mm microphones was placed on the ground 11.6 m from the centerline of the jet axis. As shown in the left plot of Figure 4, the ground array element spacing was 0.61 m, and the array spanned 30 m. Following standard practices, the angles shown in the measurement schematic are measured relative to the engine inlet and the maximum array reference point (MARP), $z = 5.5$ m in the left plot of Figure 4. It is important to note that these angles, hereafter referred to as γ, are the supplementary angles of the angles θ used in Sec. II.

The ground array recorded each engine condition 90 times. Each noise measurement was taken for 30 seconds at either a 48 kHz or 96 kHz sampling rate, depending on the engine condition tested, and each resultant waveform was divided into time-waveform blocks of 2^{15} samples each with 50% overlap. The right plot of Figure 4 show the average overall sound pressure levels (OASPL) across the ground array at each engine power, along with the standard deviations. A detailed description of the experiment is found in Wall *et al.*,[19] and Neilsen *et al.*[29] contains the spectral variation of the measured sound as a function of angle along the ground array.

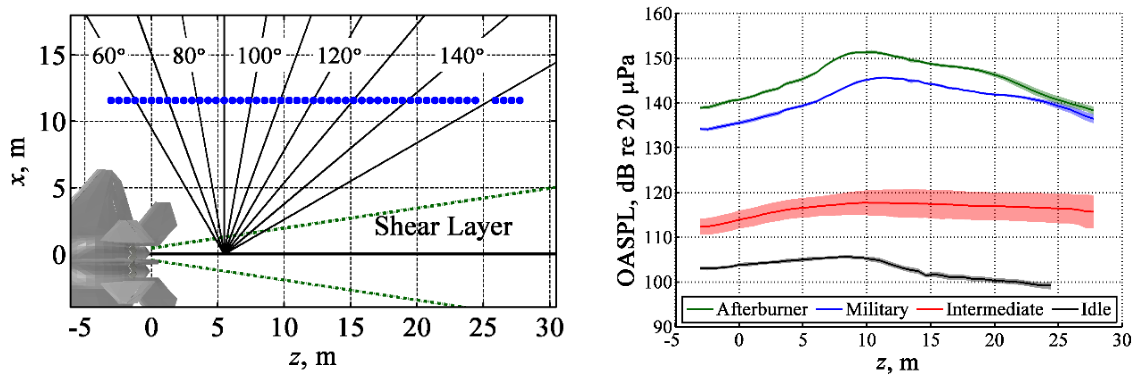

Figure 4. Experimental Setup. *(Left) Schematic of noise measurements of a tethered high-performance military aircraft. The blue dots represent the locations of the 50-microphone ground array located 11.6 m to the sideline of the jet centerline. Angles, γ, are measured relative to the engine inlet and the microphone array reference point at $z = 5.5$ m. (Top) Overall sound pressure levels (OASPL) across the ground array. The dark line for each color is the average over the measurements, and the shaded region indicates +/- one standard.*

A. Level-Educed Wavenumber Spectra

The ground array in the vicinity of the F-22 is used, as described by Morris,[16] to obtain azimuthally averaged, scaled amplitudes of the axial wavenumber spectra as a function of frequency at different engine conditions. The first step is to decompose the one-third-octave band levels on the 50 ground-based microphones into portions that match the large-scale and fine-scale similarity spectra (LSS and FSS as in Tam *et al.*[22]). The spatial distribution of the LSS levels is then used as $S(R,\theta,\omega)$ to estimate the scaled amplitudes of the axial wavenumber spectrum, $A_j G_0(k_z,\omega)/D_j$, as the square root of Eq. (11) as outlined in Sec. II.A. While the spectral decomposition process has some inherent uncertainty, it provides an estimate for the azimuthally averaged wavenumber spectrum of the wavepacket associated with the pressure fluctuation on a cylinder of radius $r_0 = D_j/2$ concentric with the jet axis.

As noted by Morris,[16] there is a bit of latitude in choosing the parameters that provide the best fit between the measured spectra and the LSS and FSS similarity spectra. In this case, two guidelines were applied. First, although some studies have used the entire spectrum (20 Hz-20 kHz) in matching the similarity spectra, the decompositions presented here primarily strive for agreement in the peak frequency region (50-1000 Hz at most locations). An example of the decomposition at military power is shown in Figure 5 for four of the ground-based microphones at one-third octave (OTO) band center frequencies. More locations are shown in Neilsen *et al.,*[29] in which angles, γ, are used to indicate the location of the microphones. For sake of comparison, the angles of the four locations shown in Figure 5 are listed in the caption of Figure 5. The spectral decompositions shown here and in Ref. 29 mostly follow the trends predicted by Tam *et al.*[22] The FSS spectrum fits well at angles upstream of the maximum array reference point of 5.5 m: $\gamma = 60°$-$80°$. The LSS are representative in the maximum radiation direction ($\gamma = 120°$-$140°$) with a few exceptions: the double spectral peak in the maximum radiation direction,[29,30,36] and the high-frequency slope, which is likely due to nonlinear propagation effects.[36] The combination of the FSS and LSS produce a better match at in between angles ($\gamma = 90°$-$110°$) and aft of the maximum radiation direction ($\gamma > 150°$), the latter of which was first reported in Neilsen *et al.*[29]

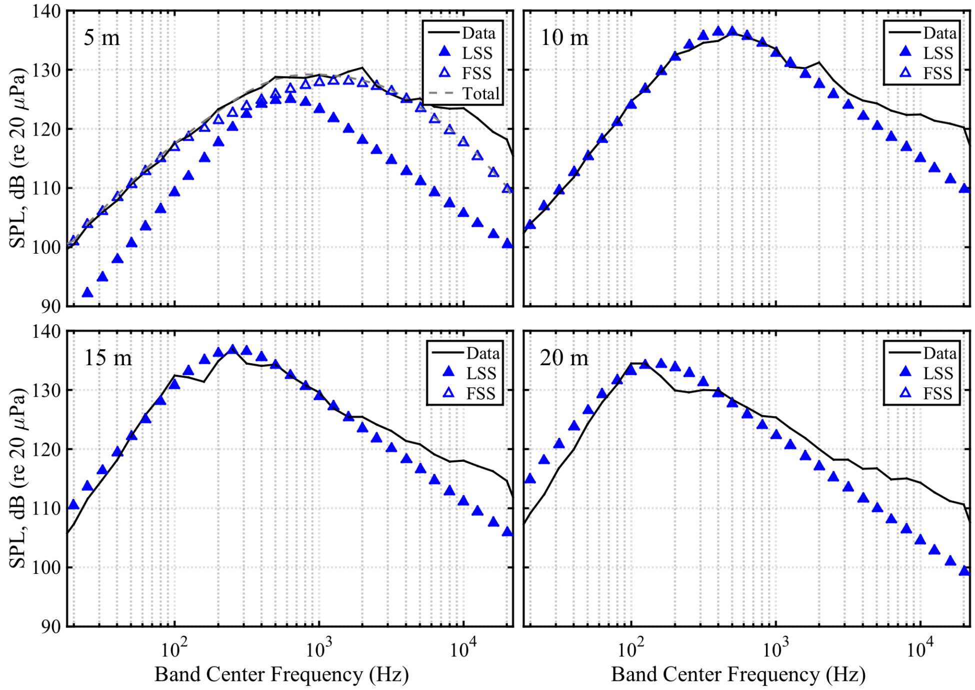

Figure 5. **Similarity spectra decomposition.** *A comparison of the measured one-third octave band spectra (black lines) for the ground-based microphones, when one engine is operated at military power, with the fine-scale and large-scale similarity spectra. At* $z = 5$ *m (*$\gamma = 87°$*), the combination of the FSS and LSS spectra yields a better match to the measured spectra. At* $z = 10$*,* 15*, and* 20 *m (*$\gamma = 110°, 130°,$ *and* $142°$*, respectively), only the LSS is used. More examples are given in Ref. 29.*

In addition to visually inspecting the spectral shapes, the OASPL associated with the FSS and LSS spectral contributions is constrained to grow or decay smoothly as a function of downstream distance. The decomposition into LSS and FSS contributions is summarized in **Figure 6**, which shows the overall level associated with each similarity spectrum as a function of downstream distance for three engine conditions: intermediate, military, and afterburner. In all three cases, the measured levels and spectral shapes are matched solely by FSS contributions for locations near and forward of the nozzle exit ($z = 0$ m). Along the array, the contribution from the LSS spectrum begins to be noticeable around $z = 2.5$ m for intermediate, 3.5 m for military power, and 6.5 m at afterburner. The measured spectral shape is matched with the LSS alone starting at $z = 13.5$ m for intermediate and approximately 8 m for military and afterburner. While the spatial distribution of FSS and LSS levels are only approximate due to the intrinsically nonunique nature of the similarity spectra matching process, their contributions to the OASPL follow reasonable trends and thus, provide a constraint to the similarity spectra fits.

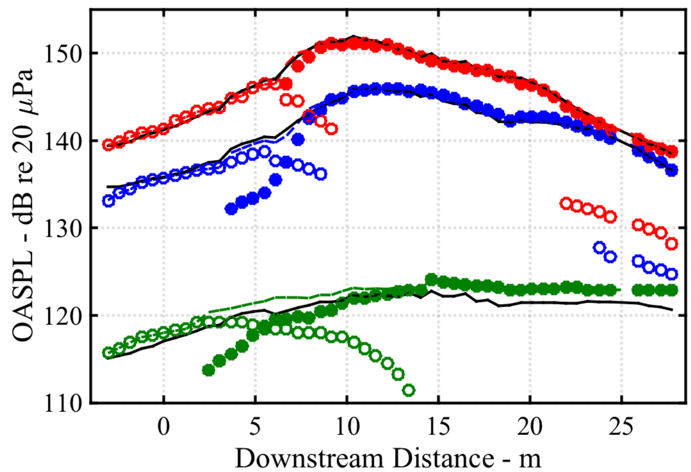

Figure 6. **OASPL of the similarity spectra decomposition.** *The OASPL contributions of the similarity spectra decomposition for the military engine condition across the 50 ground-based microphones, into LSS and FSS contributions. The open symbols represent the FSS contributions and the filled symbols the LSS contributions. The solid black line is the overall sound pressure level (OASPL) of the data at each of the 50 microphone locations, and the dashed line is the combined level from the two similarity spectra contributions.*

1. Axial Wavenumber Spectra

Using the spatial distribution of the sounds pressure levels associated with the LSS spectra, the scaled amplitudes of the axial wavenumber spectrum, $A_j|G_0(k_z,\omega)|/D_j$, are obtained following the procedure outlined in Sec. II.A. The results are shown in Figure 7 for several one-third-octave, band center frequencies for the case where a single engine is operated at military (100%) power .The wavenumbers of the data-educed spectra shown in Figure 7 correspond to only the supersonic, propagating components: $|k_z| \leq \omega/c$. Similar wavenumber amplitude plots for a laboratory-scale jet are presented in Figure 4 of Ref. 16. Although the lab-scale results are plotted versus Strouhal numbers (St), which is not possible for the F-22 case where the jet operating parameters are not available, the scaled axial wavenumbers exhibit a similar behavior. For example, at St = 0.2 for the highest jet velocity (U_j = 618 m/s) in the laboratory case, the peak in the wavenumber spectrum occurs at k_zD_j~1.9. Similarly, for the F-22 at military power, the peak in the wavenumber spectrum occurs at k_zD_j~1.7 at 250 Hz, which is near the dominant OTO band in the Mach wave radiation direction.

Other similarities between the laboratory and full-scale cases are found by examining the peak in the wavenumber spectrum. For the intermediate engine power case in Figure 7, the data-educed wavenumber spectra do not contain a peak, similar to the lower speed jets in Morris.[16] The lack of a wavenumber spectral peak indicates that these jet conditions do not permit trace wavenumber matching, and consequently, indicates a convectively subsonic peak wavenumber. For the higher-velocity jets in both the lab and the full-scale studies, more of wavenumber spectrum is convectively supersonic as frequency increases, such that the trace wavenumber matching produces efficient sound radiation at greater angles, relative to the jet centerline, at higher frequencies. Papamoschou[17] suggests that this variation in the frequency-dependent direction of Mach wave radiation accounts for the shift in peak frequency in the observed spectra as a function of angle, but then found that addition of a monopole was needed to match sideline levels.

A comparison between the military and afterburner cases in Figure 7 leads to additional insights. At all frequencies, the peaks in the military spectra occur at slightly larger values of k_z than at afterburner, which correspond to lower convective velocities for military power. In addition, the peak regions of the axial wavenumber spectra appear narrower for military than for afterburner cases. Since $G_0(k_z,\omega)$ is the Fourier transform of the wavepacket shape, a narrower spectrum in k_z corresponds with a broader distribution in z.

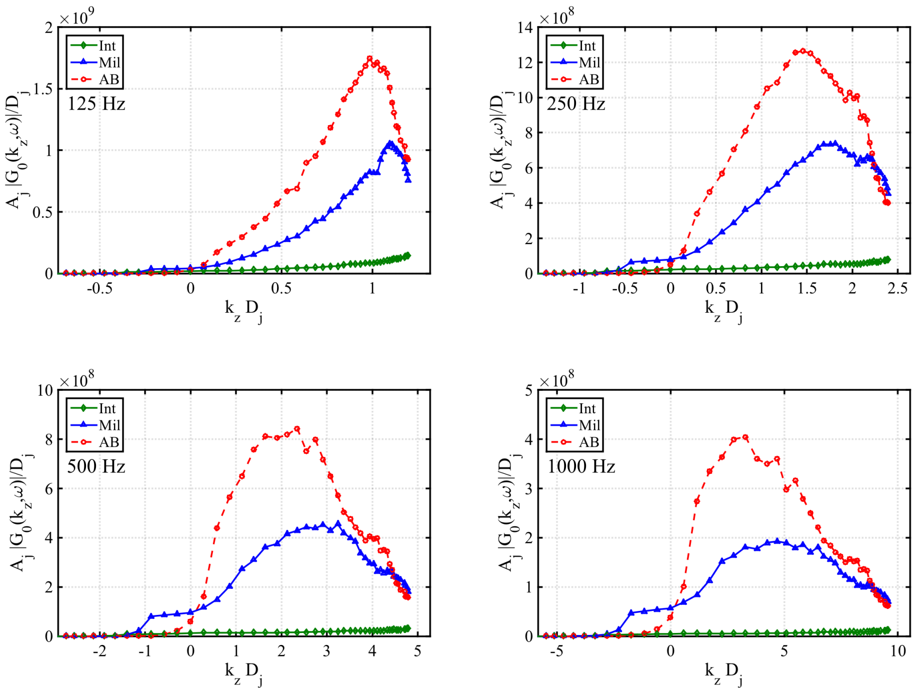

Figure 7. **Scaled, data-educed, axial wavenumber spectra** ***for 125, 250, 500, and 1000 Hz.*** *The wavenumber spectra are obtained using the LSS spectral decomposition of the aircraft noise measured of 50 ground-based microphones when one engine was operated at intermediate (green), military (blue), and afterburner (red) power.*

In addition to the prospect of sound field prediction from data-educed wavepackets, there is also the potential to obtain estimated frequency-dependent features. For example, as shown in Figure 8 for military power, the increase in width of the wavenumber spectra with frequency corroborates the idea that the wavepacket amplitude envelope contracts at higher frequencies. Also, the value of k_z associated with the peak in the spectrum, $k_{z,\mathrm{peak}}$, increases as frequency increases; this is tied to changes in the convective Mach number, similar to what was reported in Table 2 of Morris[16] and Figures 9-11 of Papamoschou.[17] The convective speed, U_c is related to the wavenumber at which the spectrum has its maximum, by $U_c = \omega/k_{z,\mathrm{peak}}$. Preliminary estimates of U_c for military engine power are listed in the legend of Figure 8, which more clearly shows the change in the wavenumber spectra with frequency. These estimated U_c values are supersonic, consistent with the strong Mach wave radiation exhibited at military power. The values of U_c are tied to the angle of maximum radiation: $\cos(\theta_{\mathrm{peak}}) = c/U_c$, where θ_{peak} is measured from the downstream axis (jet exhaust). In contrast to prior laboratory-scale studies that used far-field levels, the measurements used for this analysis were made relatively close to the aircraft. Thus, the estimates of U_c depend upon the origin of the spherical coordinate system used in obtaining the expression for the scaled wavenumber spectral amplitudes in Eq. 11. Instead of using the nozzle exit plane ($z = 0$ m), the origin at $z = 5.5$ m, as shown in **Figure 4**, is used for the results in Figure 8. This choice corresponds to what was used previously as an estimate of the apparent maximum sound generation region, and the corresponding angles concur with the observed far-field directivity.[19] These results constitute the first wavepacket-based representation of full-scale jet noise, and the U_c estimates help to provide a bridge for those doing laboratory-scale or computational work.

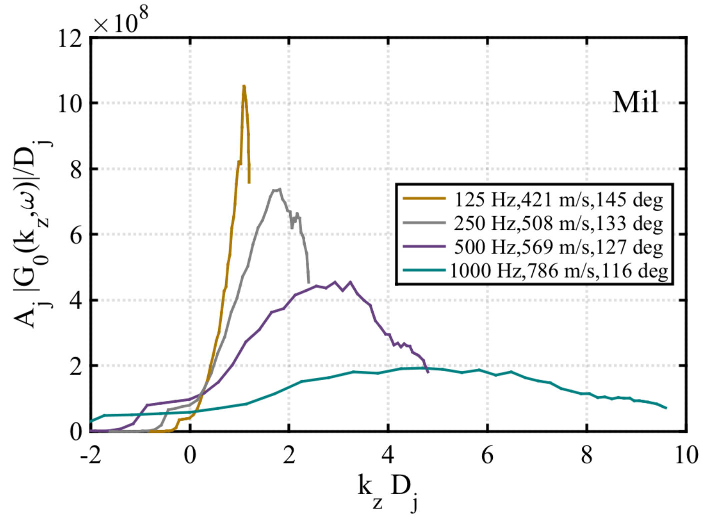

Figure 8 Frequency-dependent wavenumber spectra at military power. *Scaled, data-educed, axial wavenumber spectra as a function of frequency for the tethered F-22 with a single engine operated at military power. The estimated convective speed and corresponding angles are relative to the reference point z = 5.5 m from the nozzle exit plane, as illustrated in Figure 4.*

2. Frequency-dependent Analytical Wavepackets

The data-educed wavenumber spectra and the analytical wavepacket model from Papamoschou[17] are combined to obtain a preliminary wavepacket representation of the large-scale turbulent mixing noise from the F-22 with one engine operated at military power. Because the analytical wavepacket shape defined in Eq. (5) is problematic for $z < 0$, the analytical wavepackets are defined from the nozzle exit plane, $z = 0$. A second set of data-educed wavenumber spectra are calculated for an origin at $z = 0$ to be used in the optimizations. A simulated annealing algorithm minimizes the mismatch been the magnitudes of the normalized, data-educed wavenumber spectra and the normalized spatial Fourier transform of the analytical wavepacket model defined in Eq. (5). The cost function, E, for a set of wavepacket modeling parameters $\boldsymbol{m} = [U_c, b_1, b_2, g_1, g_2]$, minimized in the optimization is

$$E(\boldsymbol{m}) = \sum_{i=1}^{N} \left[\frac{\left|\hat{P}_0\left(k_{z,i}, \boldsymbol{m}\right)\right|}{\hat{P}_{0,\max}(\boldsymbol{m})} - \frac{\left|G_0\left(k_{z,i}\right)\right|}{G_{0,\max}} \right]^2 ,$$

where $\hat{P}_{0,\max}(\boldsymbol{m})$ and $G_{0,\max}$ are the maximum values of the analytical and data-educed wavenumber spectra, respectively, and N is the number of k_z values at which they are compared.[18] In practice, $\hat{P}_0\left(k_{z,i}, \boldsymbol{m}\right)$ and $\left|G_0\left(k_{z,i}\right)\right|$ are defined at different k_z values, so an interpolation is necessary before calculating E. As described in Sec. II.D, the cost function is most sensitive to the parameter U_c because it determines the location of the peak of the wavenumber spectrum. The parameter b_2 is also expected to influence the wavenumber spectra match more than the other modeling parameters.

To illustrate the nonuniqueness of the parameter estimates obtained by the simulated annealing algorithm,[31] a series of optimizations, each with at a different set of initial parameters, are performed and the results that yield approximately the same value of E are compared. As an example, the 250 Hz, military power, data-educed wavenumber spectrum is shown in Figure 9 along with the wavenumber amplitude spectra obtained from three optimizations. Despite having different initial and final modeling parameters the optimized wavenumber spectra have the same shape as the data-educed spectrum (upper part of Figure 9). All cases provide a consistent convective Mach number for the jet noise, which is evidenced by the ability to consistently match the peak of the wavenumber spectrum. The associated axial wavepacket shapes are plotted in the lower part of Figure 9. For the three optimizations shown, the axial wavepackets are located at different values of z, even though they have the same wavenumber spectra. This is the result of the shifting property of the Fourier transform in which a translation in z of the wavepacket shape corresponds to a phase change in the wavenumber spectrum. Thus, the exact position of the wavepacket is not identified by an optimization based on the magnitude of the wavenumber spectrum. In all three cases shown, the optimized wavepackets have the same convective speed and spatial extent and, while the rate of onset varies slightly, they have basically the same rate of decay. This is consistent with the sensitivity study in Sec. II.D, which showed that the wavenumber spectral shape depends more strongly on the value of b_2 than b_1.

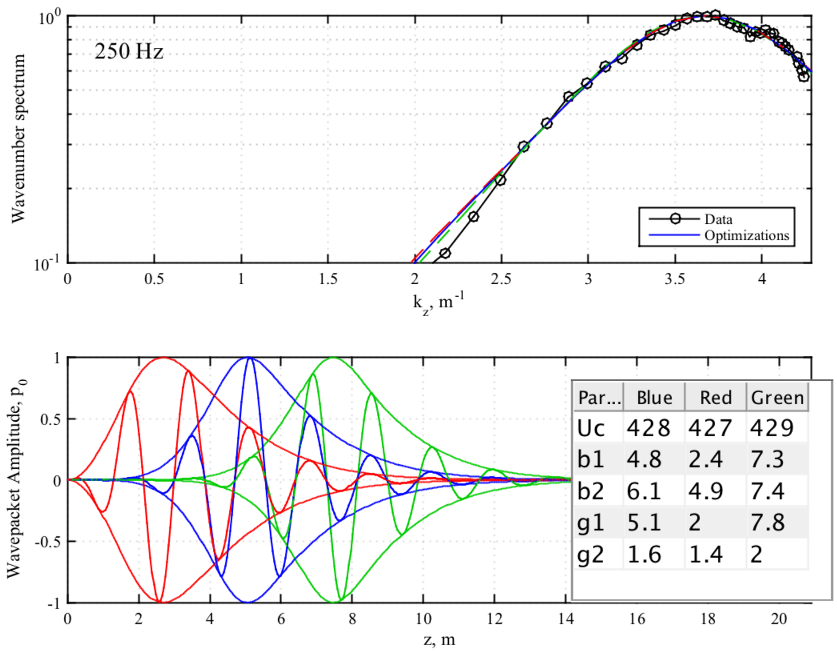

Figure 9. Example of wavepacket optimization at 250 Hz for military power. *(Upper) Analytical axial wavenumber spectral amplitudes, $\widehat{\boldsymbol{P}}_{\mathbf{0}}$, from three optimizations (colored lines), with the same cost function, and the data-educed spectrum, $\boldsymbol{G}_{\mathbf{0}}$ (black line with circles). All the spectra are normalized such their maximum value is one. (Lower) The magnitude and real parts of the axial wavepackets, $\boldsymbol{p}_{\mathbf{0}}$, based on the parameters obtained by the three optimizations, which are shown in the inset table. The cost function values, $\boldsymbol{E}$, for the three optimizations are 2.08 x 10^{-4}(blue), 2.10 x 10^{-4}(red), 2.12 x 10^{-4}(green).*

To compare the variation in axial wavepacket shapes at different frequencies, the wavepacket shapes corresponding to the optimization results at 125, 250, 500, and 1000 Hz are plotted in the left side of Figure 10, such that the peak amplitude occurs at $z = 0$ m for each frequency. Overall, the optimized wavepacket shapes show some expected features. At low frequencies, the wavepackets are considerably longer, and the spatial extent contracts as frequency increases. However, if instead of plotting the wavepackets as a function of z, they are plotted as a function of acoustic wavelength, $\lambda = c/f$, the variation with frequency is substantially reduced. It is significant that the main features of the data-educed wavenumber spectra are matched by wavepackets that extend approximately 5-6 wavelengths at each of these frequencies. However, the spatial rate of oscillations in the real part of the wavepacket does vary with frequency as it is tied to the peak in the wavenumber spectra, the convective speed, and the directivity of the sound radiation.

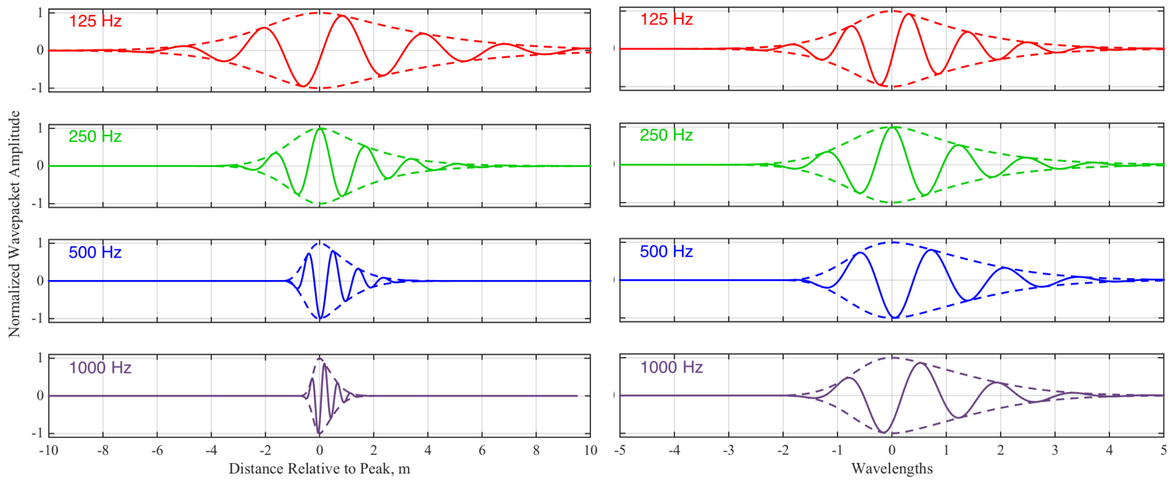

Figure 10 Optimized wavepackets at 125, 250, 500, and 1000 Hz. *(Left) The real part and magnitude of normalized axial wavepackets for the modeling parameters that yield the best agreement with the data-educed wavenumber spectra from the F-22, with one engine operated at military power, plotted as a function of distance in meters. (Right) The same wavepackets plotted as a function of acoustic wavelength.*

B. Far-field Predictions

In constructing an equivalent source representation of the turbulent mixing noise, one of the main questions is whether the single, coherent wavepacket model is sufficient to predict the radiated field. To examine this question, the wavenumber spectra from the optimized wavepackets are employed in Eq. (17). The resulting predicted field is plotted, along with the measured levels for one-third octave band center frequencies in Figure 11, where scaling factors $\epsilon(\omega)$ are used to match the peak levels. In general, the modeled field captures the general region of the Mach wave radiation. At all frequencies, the modeled field under estimates the levels for $z < 7$ m. This is not surprising since, as seen in Figure 6, the LSS contributions to the measured overall level are less than the FSS contributions for $z < 7$ m. In addition, the single, coherent, lip-line pressure wavepacket is not able to capture the dual lobe nature of the sound field, as seen at 250 Hz in Figure 6. A similar dual lobe was recently seen in CFD simulations of a heated jet.[32] At 1000 Hz, the single wavepacket underestimates the measured levels for $z > 15$ m. This is expected because the measured spectral shapes have shallower high-frequency slopes in this region due to nonlinear steepening. Although there is general agreement, these three features indicate the shortcomings of using a single coherent wavepacket and linear propagation to predict the noise levels around a military aircraft at high engine power.

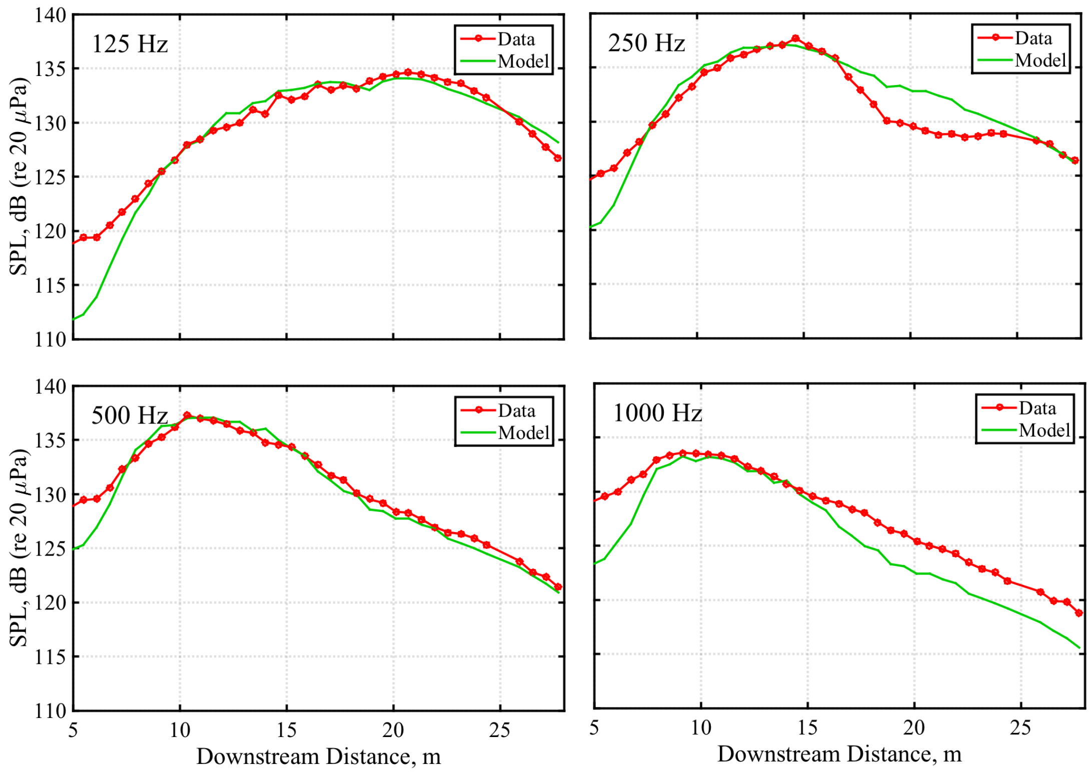

Figure 11 Comparison of measured and predicted levels. *The levels predicted by the equivalent wavepacket model (solid) are compared to levels measured on the ground-based microphones (dotted), at military power. The modeled levels are based on the optimized wavenumber spectra and the amplitude is shifted to match the peak level.*

IV. Concluding Discussion

The wavenumber eduction method described in Refs. 1, 2, and 16 has been applied to noise measured in the vicinity of a tethered, high-performance military aircraft. This methodology has yielded, for the first time, the amplitudes of the wavenumber spectra for a wavepacket representation of full-scale military jet noise. The general features in the resulting data-educed wavenumber spectra are similar to those found for a laboratory-scale jet study in Ref. 16: (1) the peak in the wavenumber spectrum is not present at intermediate engine power or lower jet velocities, indicative of a convectively subsonic conditions, and (2) the wavenumber associated with the peak in the wavenumber spectrum increases with frequency, which corresponds directly to the changes in angle at which the coherent radiation is being emitted and the corresponding increase in convective speed. In addition, a broader wavenumber spectrum at higher frequencies potentially implies a more compact wavepacket source region. It is also possible that that the data-educed wavenumber spectra contain the superposition of multiple wavepackets with varying peak wavenumbers, which is the subject of an ongoing study.[33]

Simulated annealing optimizations have been employed to minimize the difference between the data-educed wavenumber spectra for military power and the wavenumber spectra associated with the analytical wavepacket model from Papamoschou.[17] The corresponding frequency-dependent wavepacket shapes show the expected source contraction with increasing frequency when plotted vs. axial distance. However, when the axial distance is scaled by wavelength, the spatial extent of the wavepackets is not substantially different for band center frequencies spanning three octaves. The self-similar nature of the optimized axial wavepackets has not been reported previously.

The optimized wavepackets can predict the measured field with three exceptions: the dual-lobe in the maximum radiation direction, the sideline radiation, and the nonlinear steepening, none of which are included in the LSS decomposition used to obtain the data-educed wavenumber spectra. Studies into the nature of the dual spatial lobe and corresponding dual spectral peak are ongoing.[32,34-37] It is possible that the summation of mutually incoherent wavepackets could eventually model this dual-lobe phenomena. Additional efforts are needed to construct an equivalent source model that better predicts measured far-field levels to the sideline. With regard to improving the sideline match, Papamoschou in Ref. 17 added a monopole source to $S_{w,\mathrm{far}}$, which essentially adds uncorrelated noise to the model. The possibility of creating an equivalent source model that incorporates both a correlated and uncorrelated source distribution was explored by Morgan *et al.*[38] In that case, two line arrays with Rayleigh distributed amplitudes were used: the point sources on one array have a constant phase relationship derived from the far-field directivity angle, while the others have random phase relationship. Another idea is to incorporate the omnidirectional nature of the sideline radiation by including an uncorrelated, Gaussian-based, wavepacket-like model. The Gaussian parameter could be selected to fit a wavenumber decomposition of the FSS contributions to the overall levels, similar to as was done here, and in Ref. 16, with the LSS contributions. Alternatively, it is possible that the entire wavenumber spectrum of the measured levels could be used to define wavepackets models for the jet noise, instead of performing the similarity spectra decomposition.

Moving forward, a different analytical model of the axial wavepacket will be investigated for two reasons. First, of the five modeling parameters, only two, U_c and b_2, control the primary features of the wavenumber spectrum. Thus, the uncertainty in the estimates of the remaining three parameters is very large. A model with fewer parameters, all of which impact the shape of the wavenumber spectrum, needs to be employed. Second, the mathematical function is not well behaved for negative distances which, at locations close to the jet, results in difficulty in estimating convective velocity.

There are limitations in using only level-based analyses to construct an equivalent source for jet noise. First, because only the magnitudes of the data-educed wavenumber are obtained from the LSS spectral density, the location of the peak in the axial wavepackets is identified. Second, a single, coherent wavepacket cannot reproduce the complex coherence of the measured field, as explained in Harker *et al.*[33] A more complete equivalent source model needs to account for the field coherence as well as the measured levels. Such a model is needed to successfully model the noise environment of a high-performance military aircraft.

Acknowledgments

The authors gratefully acknowledge funding for this analysis from the Office of Naval Research. We thank Alan T. Wall and Trevor A. Stout for helpful discussions. This research was supported in part by the appointment of Blaine M. Harker to the Student Research Participation Program at U.S. Air Force Research Laboratory, 711 Human Performance Wing, Human Effectiveness Directorate, Warfighter Interface Branch, Battlespace Acoustics Branch administered by the Oak Ridge Institute for Science and Education through an interagency agreement between the U.S. Department of Energy and USAFRL. The measurements were funded by the Air Force Research Laboratory through the SBIR program and supported through a Cooperative Research and Development Agreement (CRDA) between Blue Ridge Research and Consulting, Brigham Young University, and the Air Force.[39] Distribution A: Approved for public release; distribution unlimited. 88ABW Cleared 12/4/2015; 88ABW-2015-5861.

References

[1] Tam, C. K. W., and Burton, D. E., "Sound generated by instability waves of supersonic flows. Part 1. Two-dimensional mixing layers," *Journal of Fluid Mechanics*, Vol. 138, 1984, pp. 249-271.

[2] Tam, C. K. W., and Burton, D. E., "Sound Generation by the Instability Waves of Supersonic Flows. Part 2. Axisymmetric Jets," *Journal of Fluid Mechanics*, Vol. 138, 1984, pp. 273-295.

[3] Jordan, P., and Colonius, T., "Wave packets and turbulent jet noise," *Annual Review of Fluid Mechanics*, Vol. 45, 2013 pp. 173-195.

[4] Tam, C. K. W., Viswanathan, K, Ahuja, K. K., and Panda, J. "The Sources of Jet Noise: Experimental Evidence," *Journal of Fluid Mechanics*, Vol. 615, 2008, pp. 253-292.

[5] Viswanathan, K., "Aeroacoustics of hot jets," *Journal of Fluid Mechanics*, Vol. 516, 2004, pp. 39-82.

[6] Reba, R., Narayanan, S., and Colonius, T., "Wave-packet models for large-scale mixing noise," *International Journal of Aeroacoustics*, Vol. 9, 2010, pp. 533-558.

[7] Reba, J., Simonich, J., and Schlinker, R., "Sound Radiated by Large-Scale Wave-Packets in Subsonic and Supersonic Jets," AIAA Paper 2009-3256, May 2009.

[8] Mollo-Christensen, E., "Jet noise and shear flow instability seen from an experimenter's viewpoint," *Transactions of ASME: Journal of Applied Mechanics*, Vol. 34, 1967, pp. 1-7.

[9] Tinney, C.E., Ukeiley, L.S. & Glauser, M.N., "Low-dimensional characteristics of a transonic jet. Part 2. Estimate and far-field prediction," *Journal of Fluid Mechanics*, Vol. 615, 2008, pp. 53–92.

[10] Suzuki, T. and Colonius, T., "Instability waves in a subsonic round jet detected using a near-field phased microphone array," *Journal of Fluid Mechanics,* Vol. 565, 2006, pp. 197-226.

[11] Suzuki, T. "Coherent noise sources of a subsonic round jet investigated using hydrodynamic and acoustic phased-microphone arrays," *Journal of Fluid Mechanics,* Vol. 730, 2013, pp. 659-698.

[12] Kerherve, F., Guitton, A., Jordan, P., Delville, J., Fortune, V., Gervais, Y. & Tinney, C., "Identifying the dynamics underlying the large-scale and fine-scale jet noise similarity spectra," AIAA Paper 2008-3027, 2008.

[13] Tinney, C.E. & Jordan, P., "The near pressure field of co-axial subsonic jets," *Journal of Fluid Mechanics*, Vol. 611, 2008, pp. 175–204.

[14] Reba,R. J. Simonich and R. Schlinker, "Measurement of Source Wave-Packets in High-Speed Jets and Connection to Far-Field Sound," AIAA Paper 2008-2891, May 2008.

[15] Koenig M, Cavalieri, A. V. G., Jordan, P., Delville, J., Gervais Y., and Papamoschou, D., "Farfield filtering and source imaging of subsonic jet noise," *Journal of Sound and Vibration*, Vol. 332, No. 18, 2013, pp. 4067–4088.

[16] Morris, P. J., "A note on noise generation by large scale turbulent structures in subsonic and supersonic jets," *International Journal of Aeroacoustics*, Vol. 8, No. 4, 2009, pp. 301–315.

[17] Papamoschou, D., "Wavepacket Modeling of Jet Noise Sources," AIAA Paper 2011-2835, 2011.

[18] Papamoschou, D., "Prediction of Jet Noise Shielding," AIAA Paper 2010-0653, 2010.

[19] Wall, A. T., Gee, K. L., James, M. M., Bradley, K. A., McInerny, S. A., and Neilsen, T. B., "Near-field noise measurements of a high-performance military jet aircraft," Noise Control Eng. J. **60**, 421-434 (2012).

[20] Tam, C. K. W. and Chen, K. C., "A statistical model of turbulence in two dimensional shear layers," *Journal of Fluid Mechanics*, Vol. 92, 1979, pp. 303-326 .

[21] Tam, C. K. W., "Stochastic model theory of broadband shock associated noise from supersonic jets," *Journal of Sound and Vibration*, Vol. 116, 1987, pp. 265-302.

[22] Tam, C. K. W., Golebiowsky, M. and Seiner, J. M., "On the Two Components of Turbulent Mixing Noise from Supersonic Jets," AIAA Paper 96-1716, 1996.

[23] Tam, C. K. W. and Zaman, K., "Subsonic Noise from Nonaxisymmetric and Tabbed Nozzles," *AIAA Journal*, Vol. 38, 2000, pp. 592–599.

[24] Tam, C. K. W., Pasouchenko, N. N., and Schlinker, R. H., "Noise source distribution in supersonic jets," *Journal of Sound and Vibration*, Vol. 291, 2006, pp. 192-201.

[25] Viswanathan,K., "Analysis of the two similarity components of turbulent mixing noise," *AIAA Journal*, Vol. 40, 2002, pp. 1735–1744.

[26] Viswanathan, K., "Does a Model-Scale Nozzle Emit the Same Jet Noise as a Jet Engine?" *AIAA Journal*, Vol. 46, 2008, pp. 1715-1737.

[27] Viswanathan, K., and M. J. Czech, "Role of jet temperature in correlating jet noise," *AIAA Journal*, Vol. 47, 2009, pp. 1090-1106.

[28] Schlinker, R. H., Liljenberg, S. A., Polak, D. R., Post, K. A., Chipman, C. T., and Stern, A. M., "Supersonic Jet Noise Source Characteristics & Propagation: Engine and Model Scale," AIAA Paper 2007-3623, May 2007.

[29] Neilsen, T. B., Gee, K. L., Wall, A. T., and James, M. M., "Similarity spectra analysis of high-performance jet aircraft noise," *Journal of the Acoustical Society of America*, Vol. 133, No. 4, 2013, pp. 2116-25.

[30] Neilsen, T. B., Gee, K. L., Wall, A. T., James, M. M., and Atchley, A. A., "Comparison of supersonic full-scale and laboratory-scale jet data and the similarity spectra for turbulent mixing noise," *Proceedings of Meetings on. Acoustics,* Vol. 19, 2013, paper 040071.

[31] Corte, H., "Simulated Annealing," Matlab Central. Last viewed 18 Dec 2015.
http://www.mathworks.com/matlabcentral/fileexchange/33109-simulated-annealing-optimization

[32] Liu, J., Corrigan, A., Kailasanath, K., Taylor, B., "Impact of the specific heat ratio on the noise generation in a high-temperature supersonic jet," AIAA Paper 2016-2125, January 2016.

[33] Harker, B. M., Gee, K. L., Neilsen, T. B., Wall, A. T., and James, M. M., "Wavepacket modeling and full-scale military jet noise beamforming analyses," AIAA Paper 2016-2129, January 2016.

[34] Tam, C. K., and Parrish, S., "Noise of high-performance aircrafts at afterburner," *Journal of Sound and Vibration,* Vol. 352, 2015, pp. 103–128.

[35] Stout, T. A. , Gee, K. L., Neilsen, T. B., Wall, A. T., Krueger, D. W., and James, M. M., "Preliminary Analysis of Acoustic Intensity in a Military Jet Noise Field," *Proceedings of Meetings on Acoustics*, Vol. 19, 2013, paper 040074.

[36] Neilsen, T. B., Gee, K. L., and James, M. M., "Spectral characterization in the near and mid-field of military jet aircraft noise, AIAA paper 2013-2191, 2013.

[37] Wall, A. T., Gee, K. L., Neilsen, T. B., and James, M. M.,"Acoustical holography imaging of full-scale jet noise fields," *Proceedings of Noise-Con*, Denver, CO, August 26-28, 2013.

[38] Morgan, J., Neilsen, T. B., Gee, K. L., Wall, A. T., and James, M. M., "Simple-source model of high-power jet aircraft noise," *Noise Control Engineering Journal*, Vol. 60, 2012, pp. 435-449.

[39] SBIR DATA RIGHTS - (DFARS 252.227-7018 (JUNE 1995)); Contract Number: FA8650-08-C-6843; Contractor Name & Address: Blue Ridge Research and Consulting, LLC, 29 N Market St, Suite 700, Asheville NC; Expiration of SBIR Data Rights Period: March 17, 2016 (Subject to SBA SBIR Directive of September 24, 2002).